Magnetic resonance imaging analysis of left ventricular function in normal and spontaneously hypertensive rats

R. G. Wise*, C. L.-H. Huang†, G. A. Gresham*, A. I. M. Al-Shafei*†, T. A. Carpenter* and L. D. Hall*

**Herchel Smith Laboratory for Medicinal Chemistry, University of Cambridge, School for Clinical Medicine, Robinson Way, Cambridge CB2 2PZ and † The Physiological Laboratory, Downing Street, Cambridge CB2 3EG, UK*

(Received 7 May 1998; accepted after revision 9 September 1998)

1. We have used magnetic resonance imaging (MRI) to examine acute morphological changes in the left ventricle throughout the cardiac cycle in normal Wistar Kyoto rats (WKY) and also to follow the development of chronic changes in spontaneously hypertensive rats (SHR). This involved the development of MRI and quantitative analysis techniques for characterizing contractile changes during the cardiac cycle.

2. Images of the cardiac anatomy in two age groups (8 and 12 weeks old) of young anaesthetized adult normal WKY and SHR were acquired in planes both parallel and perpendicular to the principal cardiac axis.

3. Complete coverage of the heart by imaging planes was achieved with high time resolution (13 ms), with typically 12 time frames in the cardiac cycle, using a short echo time (5 ms) multislice gradient-echo imaging sequence. Imaging was synchronized to the R wave of the electrocardiogram.

4. The image slices could be reconstructed into complete geometrically and temporally coherent three-dimensional data sets. Left ventricular (LV) volumes were thus reconstructed throughout the cardiac cycle by combining transverse cardiac image sections. This volume analysis revealed structural and functional differences between the normal WKY and SHR in both age groups of 8 and 12 weeks. Measurements from the cardiac images were additionally validated against histological measurements.

5. The SHR showed a raised LV end-systolic volume and a correspondingly poorer ejection fraction as well as LV hypertrophy when compared with the controls. Left ventricular function in the SHR appeared stable between the two age groups.

6. We developed a simple geometrical model of the left ventricle based on a single longitudinal image section and successfully used this to describe some functional parameters of the left ventricle in the WKY and SHR. This geometrical model has the potential to greatly reduce the imaging time needed to study the beating heart in future serial investigations of cardiac physiology in rats.

7. Our experimental and analytical methods together form a powerful set of quantitative techniques which combine both imaging and functional analysis and will be applicable for future studies of chronic physiological changes in animal disease models.

Magnetic resonance imaging (MRI) has proved invaluable for clinical cardiological investigation. However, MRI may also prove to be an important physiological tool since it combines minimal invasiveness with good measurement precision (Mohiaddin & Longmore, 1993). Furthermore, it offers good soft tissue contrast and can provide three-dimensional visualization of entire organs, permitting the use of image planes with unrestricted orientation, unlike other techniques such as ultrasound (Schnittger *et al.* 1982). MRI has been used to examine human left ventricular (LV) contraction (Underwood *et al.* 1986; Semelka *et al.* 1990; Baldy *et al.* 1994) and to evaluate LV wall and chamber volumes (Underwood *et al.* 1985; Longmore *et al.* 1985*a*,*b*; Rehr *et al.* 1985; Sechtem *et al.* 1987; Forbat *et al.* 1994), including characterization of chronic physiological changes, such as LV hypertrophy (Soldo *et al.* 1994).

There has been increasing interest in the investigation of animal models of cardiac pathology in small mammals using MRI techniques in combination with conventional analytical and histological investigations (Manning *et al.* 1990; Rudin *et al.* 1991; Rose *et al.* 1994; Laurent *et al.* 1995; Rehwald *et al.* 1997; Franco *et al.* 1997; Lorenz *et al.* 1997; Slawson *et al.* 1997). Some of those studies examine functional parameters of the left ventricle; typically images are acquired in synchrony with the R wave of an electrocardiographic (ECG) signal. Other MRI studies in humans and animals have sought to describe heart wall deformations during the cardiac cycle by velocity encoding or tagging methods (Axel & Dougherty, 1989; Decrespigny *et al.* 1991; Young & Axel, 1992). This paper applies MRI methods and methods of data analysis to cardiac changes in two rat strains, normal Wistar Kyoto rats (WKY) and spontaneously hypertensive rats (SHR) (Yamori, 1984). Animal systems offer convenient models to study chronic physiological changes in characterized genetic disease strains that may replicate human disease (Bishop, 1980).

Hypertension is a known major risk factor for cardiovascular disease. MRI examination of the heart of such an animal model of hypertension might provide insights into the physical changes and quantify the chronic physiological changes associated with it over extended periods of time. Use of MRI may help to reveal relationships between the development of hypertension and remodelling of the shape and structure of the heart and the effects of pharmacological intervention on these. The SHR strain is a widely used animal model for hypertension (Bishop, 1980; Yamori, 1984) and offers significant advantages over humans for the study of pathophysiological changes. The strain is readily available and develops pathology over a considerably more rapid time course than does the human. The hypertension is present in many SHR by as early as 5 weeks of age (Bishop, 1980) and typically the systolic blood pressure exceeds 200 mmHg (Bishop, 1980; Laurent *et al.* 1995) compared with around 150 mmHg in the normal WKY. In addition, the geometry of the left ventricle of the rat is much simpler than that of the human (Greenbaum *et al.* 1981), which facilitates quantitative analysis of cardiac structure in the rat.

We have developed an MRI protocol for imaging the rapidly beating rat heart and in this paper use it to compare the left ventricular function of the normal WKY with that of the SHR. Furthermore, a simple model of the left ventricle was developed which aimed to describe its function using a much reduced set of imaging planes (Underwood *et al.* 1988; Cranney *et al.* 1990). Such a model may have a wider applicability for cardiac imaging in rats by allowing imaging times to be significantly reduced. This is important because although the animals in this study were robust under anaesthetic, other animal models of cardiac pathology may require reduced imaging times for successful imaging.

METHODS

Physiological protocols

The experiments were performed on a total of 16 male rats ranging in weight from 203 to 334 g. Wistar Kyoto rats (WKY, $n = 8$), served as controls for comparison with spontaneously hypertensive rats (SHR, $n = 8$) (Harlan, UK). Each group of eight animals was subdivided into two age-matched categories of 8 and 12 weeks old, resulting in four animals of each strain in each age category. This made it possible to study the early pathology in young adult rats but with the age gap between the groups allowing observation of developments in the disease. The young age of the animals facilitated MRI examination and adminstration of anaesthetic since their body weight remained modest (typically 270 g). Table 1 summarizes the mean weight of each group. The rats were anaesthetized using 1–2% halothane in oxygen and then, soon after, systolic blood pressures were measured using the tail cuff method (Harvard Apparatus, Edenbridge, Kent, UK). Table 1 displays these systolic blood pressure values for the animals divided according to strain and age group. This tail cuff blood pressure measurement was repeated immediately after the MRI study to confirm that the systolic blood pressure remained constant within reasonable physiological limits after the onset of anaesthesia a few hours earlier. Typically, the systolic blood pressure measurement after the MRI study was slightly lower than, but within 15–20 mmHg of, the measurement taken soon after the induction of anaesthesia.

Before magnetic resonance imaging, electrocardiogram (ECG) monitoring of the animal using shielded subcutaneous leads (Sibson *et al.* 1993) was established. This subsequently enabled image acquisition to be synchronized or gated to the QRS complex of the electrocardiogram. The animal was then placed within a half sine-spaced birdcage radio frequency (RF) probe (Ballon *et al.* 1990), an oscillating circuit which was tuned to the frequency of the proton resonance (83·6 MHz). The probe was approximately half-cylindrical in shape, with an internal diameter of 4·5 cm and a length of 14 cm, and with open ends. It was oriented axially in the bore of the magnet when in use, with the animal lying within the half-cylinder. On the outer surface of the polymethylmethacrylate (PMMA) half-cylinder and running parallel to its axis were copper struts spaced sinusoidally around the circumference to generate a relatively uniform oscillating transverse magnetic field in the probe. This provides reasonably homogeneous transmission and reception of RF power and thus signal intensity over the cardiothoracic cavity of the animal. Attached to the outside of the probe were capacitors for tuning its resonant circuit and a copper loop of 3 cm diameter to inductively couple the resonator to a coaxial cable for transmission and reception of RF. Surrounding this assembly was an RF shield consisting of a cylinder of copper gauze (diameter 14 cm) with open ends. This type of open design of RF probe (half-birdcage) was versatile, allowed different sizes of experimental animal to be imaged and provided easy access for the animal which would not be the case with an enclosed birdcage RF probe. The animal RF probe was part of a self-contained unit that included secure attachments for ECG leads and allowed the delivery and withdrawal of gaseous anaesthetic mixtures. These measures allowed physiological monitoring of the anaesthetized animal while it was in the bore of the magnet and ensured a consistent delivery of anaesthetic gases. They also enabled repeatable positioning of the animals in different imaging sessions. Once in the probe, the animal was transported to the MRI system for imaging.

Table 1. Major cardiac parameters for the WKY and SHR groups

	WKY						SHR					
	All ages $n = 8$		8 week $n = 4$		12 week $n = 4$		All ages $n = 8$		8 week $n = 4$		12 week $n = 4$	
	Mean	S.E.M.	Mean	S.E.M.	Mean	S.E.M.	Mean	S.E.M.	Mean	S.E.M.	Mean	S.E.M.
Body weight (BW) (g)	249	15	214	9	284	13	277	14	246	9	307	13
LV myocardial volume by MRI (LVMV) (μl)	476	26	429	30	523	28	646*	22	608	6	684	35
LVMV/BW (μl g^{-1})	1·92	0·05	2·00	0·07	1·84	0·04	2·36*	0·09	2·48	0·10	2·24	0·09
End-diastolic volume (μl)	397	31	331	21	463	36	414	20	374	22	455	19
End-systolic volume (μl)	157	18	119	13	195	20	210†	8	196	9	224	9
Ejection fraction	0·61	0·02	0·64	0·03	0·58	0·01	0·49*	0·02	0·47	0·04	0·51	0·01
Systolic blood pressure (mmHg)	150	2	151	4	150	2	200*	11	177	10	216	7

Data are presented for the combined age groups of each strain, as well as for each age group separately. The left ventricular (LV) myocardial volume measured by MRI, for each individual rat, was taken from the average value from all the time points sampled in the cardiac cycle. The functional cardiac parameters were established from the transverse cardiac sections. Values quoted are the means and the standard error of the mean (S.E.M.). * $P < 0·001$ *versus* control WKY for both age groups combined. † $P < 0·05$ *versus* control WKY for both age groups combined.

After the magnetic resonance imaging examinations, the animal was killed by an intraperitoneally injected overdose (400 mg kg^{-1}) of sodium pentobarbitone (Euthatal, Rhone Merieux Ltd, Harlow, Essex, UK), followed by exsanguination (Schedule One method – Animals Scientific Procedures Act 1986). The hearts were excised and fixed in neutral buffered formalin for later examination. After fixation, the heart was trimmed to leave the LV muscle which was weighed and compared with the MRI-derived LV muscle volume.

Magnetic resonance imaging

Images were acquired in synchrony with the R wave of the ECG. Cardiac anatomy was examined throughout the cardiac cycle using imaging slices that were both parallel and perpendicular to the principal cardiac axis. This was achieved for the high intrinsic heart rates in rats; a maximum heart rate of 370 beats min^{-1} was seen in this study.

Experiments were performed in a magnetic field of 2 Tesla in an Oxford Instruments superconducting magnet with a horizontal internal bore of 31 cm. This was connected to a Bruker MSL100 console, converted to run Tomikon imaging software (version 890601, Bruker Medzin Technik GmbH, Karlsruhe, Germany) by the addition of shaped waveform generators and extra memory. The imaging gradients were produced using conventional Maxwell and Golay coils wound on a former of internal diameter 15 cm; each gradient axis was powered by two Techron 7560 and 7570 amplifiers (Crown International Inc., Elkhart, IN, USA) arranged in a series slave/master configuration (Carpenter *et al.* 1989). The RF coil was a home-built half-sine-spaced birdcage probe (Ballon *et al.* 1990) of internal diameter 4·5 cm.

Images were obtained using a multislice gradient-echo sequence, with an echo time of approximately 5 ms. The short echo time reduced motion artifacts in the images and gave a higher signal intensity for blood in the heart than for muscle, during systole. Signal loss from the blood was increased during systole when tests were carried out with longer echo times. This may be the result of turbulent blood flow.

The field of view employed was typically 4·0–5·0 cm depending on the size of the animal. A flip angle of 90 deg was achieved using a 2·5 ms Hermite pulse; this was found to give acceptable contrast. The image matrix was 128 pixels square giving a nominal pixel resolution of 390–310 μm and for display the images were zero-padded to 256 pixels square. Typically 12 image slices were acquired contiguously covering the whole left ventricle from its aortic outflow to the apex, with slice thicknesses between 1·25 and 2·0 mm (transverse slices) in different animals. The typical slice thickness was 1·4 mm for transverse cardiac slices and 1·1 mm for longitudinal cardiac slices. A full set of image slices was acquired for each subject, both in planes transverse and parallel to (longitudinal slices) the principal cardiac axis.

The effective repeat time was approximately 400 ms, depending on the heart rate of each animal; image acquisition was gated from every alternate heart beat rather than imaging every cardiac cycle. This manoeuvre reduced the incidence of gating timing errors; the cardiac period approached the imaging period of just over 151 ms in some animals. Such errors arose from triggering from voltages induced in the ECG cables by gradient switching during imaging. This regime also gave an acceptable signal from the myocardium, allowing clear visualization of the epicardial border.

Consistent image slice positioning

To perform a study in which the entire rapidly beating rat heart was imaged throughout the whole cardiac cycle and in which data sets between different animals could be compared, a repeatable and consistent image slice positioning protocol was employed. In particular, to allow subsequent quantitative analysis of the images acquired, the images were obtained through a consistent set of geometrical planes relative to the principal cardiac axis (Fig. 1*A* and *B*). This was defined by the line that joins the aortic valve and the apex of the left ventricle. Examples of the images acquired through consistent geometrical planes are displayed in Figs 2 and 3. This slice positioning protocol was a further development of the procedures introduced by Crowley *et al.* (1997) to ensure rigorous

positioning of imaging planes. The present study adopted slice positioning procedures which allowed for the fact that the principal cardiac axis was aligned at a small angle to the craniocaudal axis of each animal in both the longitudinal and sagittal planes.

The slice positioning was carried out using the following protocol:

(1) The animal was positioned horizontally in the bore of the magnetic resonance imaging gradient set, lying prone with its craniocaudal axis along the main field axis of the superconducting magnet.

(2) Sagittal images of the thoracic cavity were obtained, in a multislice data set, with a larger image field of view (typically 7 cm) than that used subsequently to acquire the complete data sets. A single sagittal pilot image is displayed in Fig. 1*A*.

(3) Using the sagittal images as a guide, the animal was then repositioned along the main field axis of the magnet to optimize its craniocaudal position relative to the RF probe, if necessary, and the sagittal images of step (2) were repeated.

(4) Using the sagittal image showing the clearest representation of the heart as a pilot image (Fig. 1*A*), transverse–coronal multislice images were positioned in a plane perpendicular to the sagittal pilot.

(5) These images showed how the principal cardiac axis was oriented in the transverse–coronal plane (Fig. 1*B*). This is a plane at an angle (established by the piloting procedure) between the transverse and coronal orientations. Using the transverse–coronal pilot image, a definitive set of typically 12 imaging planes (*transverse cardiac slices* or *sections*) was positioned perpendicular to the principal cardiac axis, covering the whole left ventricle (Figs 1*B* and 3). This formal procedure ensured that, unlike in earlier studies (Crowley *et al.* 1997), sections fell truly perpendicular to the principal cardiac axis.

(6) After acquisition of the transverse cardiac slices, one of these, showing the heart at its widest point (such as in Fig. 3), was used to select longitudinal image planes parallel to the principal cardiac axis and perpendicular to the transverse cardiac slices. They were rotated about the principal cardiac axis until positioned such that the left and right ventricles could be visualized together at their widest points (Fig. 2). The experiments typically obtained 12 *longitudinal cardiac slices* or *sections* covering the entire heart.

Temporal synchronization of image acquisition

The data acquisition in each cardiac cycle began with the first image in the time series acquired 8 ms after the triggering from the ECG R wave. The subsequent images were obtained at, typically, 13 ms intervals after the R wave, giving good time resolution throughout the cardiac cycle. Image slices in the multislice image data set were typically acquired at 12 cardiac time points. Thus the images spanned from end-diastole through end-systole and into diastole, most of the cardiac cycle.

A cycled multislice approach to image acquisition was adopted to yield each of n image slices at many time points of the cardiac cycle (Crooks *et al.* 1984; Pettigrew, 1989). Typically 12 scans were acquired, one for each image slice, for each imaged cardiac cycle.

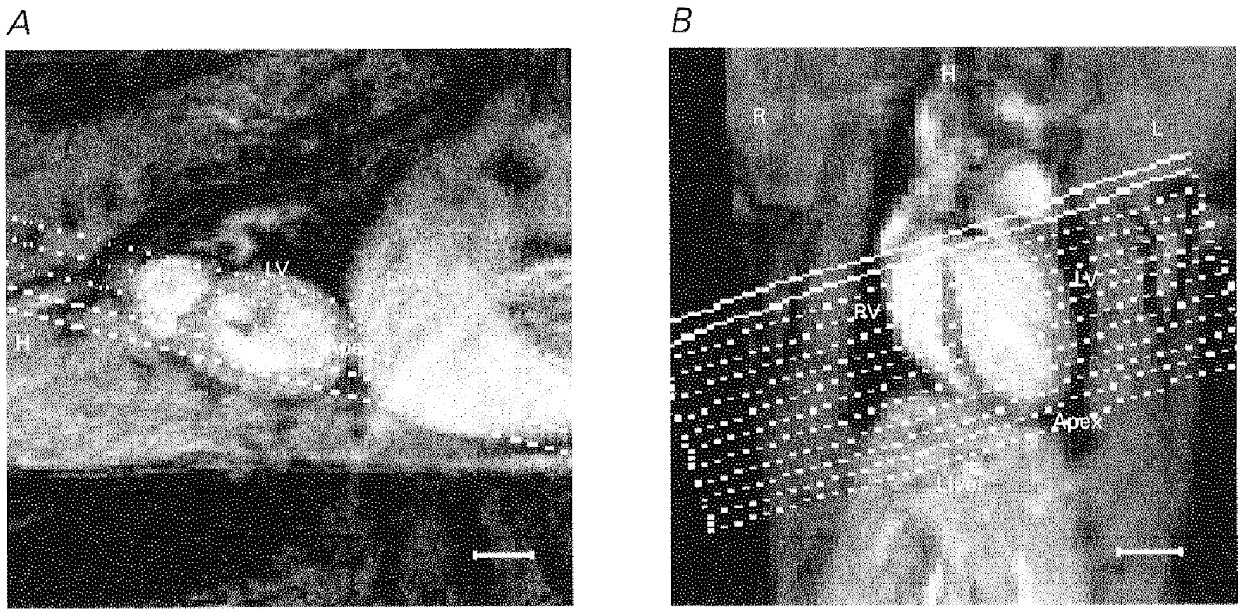

Figure 1. Pilot images

Sagittal (*A*) and transverse–coronal (*B*) pilot images used to establish the cardiac axes and to position the transverse cardiac sections used in the subsequent image analysis. The location of the liver (Liver), left and right ventricles (LV, RV) and the heart apex (Apex) are labelled, as well as the left (L), right (R) and head (H) directions. *A*, the sagittal pilot MR image showing the orientation of transverse–coronal multislice sections lying parallel to the long axis of the left ventricle (principal cardiac axis) in the plane of the image. *B*, the resulting transverse–coronal image showing the left and right ventricles most clearly and illustrating the orientation of the principal cardiac axis. The definitive set of 12 cardiac sections is positioned perpendicular to this axis. The scale bars indicate 5 mm. MR pilot images were acquired using the multislice gradient-echo imaging sequence (echo time = 5 ms) with the following parameters: field of view 5 cm for *A* and 7 cm for *B*; slice thickness 2 mm; matrix 128 square; repeat time approximately 400 ms.

The spatial ordering of image slices was interleaved with respect to the order of signal acquisition to reduce the effects of out-of-slice excitation in neighbouring slices. The multislice excitation order was cyclically rotated after collection of signals for all of the phase encode points of the image matrix. This resulted in imaging of each of the n slices at n phases of the cardiac cycle.

Each experimental run began and ended with identical multislice image data sets, bracketting each complete image data set, consisting of all slices at all imaged time points. The technique of cyclic rotation of the multislice acquisition order facilitated this manoeuvre. Images obtained at the outset and completion of each experimental run were compared to confirm that differences were minimal, hence showing that the animal was stable throughout the imaging. These precautions ensured clear and consistent images in both transverse and longitudinal cardiac section of the entire left ventricle throughout the cardiac cycle, with good temporal resolution even in the rapidly beating rat heart.

Using this protocol, the total imaging time depends on the R–R interval of the anaesthetized animal. The time required to obtain 12 different image slices each at 12 different times during the cardiac cycle, giving complete coverage of the heart, was approximately 22 min, based on two signal averages. The heart rate of the animal was followed throughout each imaging session and typically showed little variation during the acquisition of each complete image data set: this was important for the integrity of the data sets.

Image analysis of cardiac sections

Data were transfered from the Bruker Aspect computers to UNIX work stations by means of in-house hardware and software. The images were analysed by interactively defining the endocardial and epicardial borders of the left ventricle in each transverse image slice, using in-house software based on the CaMReS libraries (CaMReS, Dr N. J. Herrod, University of Cambridge, UK). The image slices covered the whole left ventricle from apex to aortic outflow. Empirical LV volumes throughout the cardiac cycle, both epi- and endocardial, were computed from the area enclosed by each border and the interslice distance, using a simple rectangular integration scheme.

We observed a considerable degree of symmetry in the shape of the left ventricle of both the WKY and SHR (Figs 2 and 3). This led to the development of a geometrical description or model of the left ventricle based upon a single longitudinal image section. This longitudinal section, acquired as part of a multislice data set, using the protocol described above, was taken from the widest part of the left ventricle and ran squarely through the right ventricle, in a similar manner to the sections of Fig. 2. At all of the imaged time points in the cardiac cycle, the epi- and endocardial borders of the left ventricle were defined in this slice. A least squares fitting procedure (in-house software written in C running on UNIX work stations) was applied to find the ellipse of best fit describing each border. The volume bounded by rotating each of these ellipses about the axis corresponding to the longitudinal axis of the heart gave a measure of the epi- and endocardial LV volumes. These volumes were compared with those derived empirically (see Results).

Results are expressed as means ± S.E.M. Student's t test was used for single comparisons between means and the statistical differences for compared means (Table 1) were considered significant at $P < 0{\cdot}05$. Least squares linear regression was used to examine linear relationships between measured or calculated quantities, with 68·3% confidence intervals quoted for the slope and y-intercept of the regression line. Correlations were quantified by Pearson's correlation coefficient denoted by r.

RESULTS

Cardiac images in longitudinal and transverse section

Figure 2 displays typical longitudinal sections and Fig. 3 displays typical transverse cardiac sections for WKY and SHR, respectively. These sections through intact beating rat hearts were taken through the widest region of the heart, each through a single geometric plane parallel and perpendicular to the principal cardiac axis (see Methods section). The images are displayed at 12 time points throughout the cardiac cycle; the time delay after the R wave trigger at which signal acquisition occurred is indicated in each panel. Contiguous transverse and longitudinal sections were obtained at typically 12 time points throughout the cardiac cycle to enable the complete quantitative reconstruction of the LV geometry.

Figures 2 and 3 confirm that the imaging protocol provided excellent temporal resolution of cardiac geometry throughout the cardiac cycle, allowing end-diastole and end-systole to be accurately identified. The frames span approximately three-quarters of the cardiac cycle and the fact that they are separated in time by only 13 ms in part reflects the use of a short echo time of 5 ms. The first frame was acquired 8 ms after the R wave trigger, at end-diastole, and shows fully dilated left and right ventricles. Subsequent frames illustrate systole with a progressive decrease in luminal diameter and an associated thickening of the LV wall, while end-systole typically occurs after about 100 ms. The final few frames of Figs 2 and 3 show diastolic refilling of the ventricles (typically 112 ms onward) as these expand towards a size similar to that shown in the first frame.

The image planes clearly delineate the cardiac anatomy in both the WKY and SHR (Figs 2, 3 and 4), as well as the aortic outflow (Fig. 2). The cardiac walls were clearly distinguishable from the lumen of the cardiac chambers, particularly for the ventricles, and from the thoracic cavity, allowing definition of ventricular borders and subsequent quantitative analysis. The multislice imaging protocol employed gave a significant signal from the myocardium, which is important for distinguishing it from the surrounding, largely low signal intensity, thoracic cavity.

In general, during systole and very early diastole the blood shows brighter than the surrounding heart muscle in both the longitudinal and transverse cardiac sections (Figs 2 and 3). This results from inflow brightening (Pope & Yao, 1993) between successive slice excitations and the longer T_2 (transverse relaxation time constant) of blood than muscle (Beall *et al.* 1984), giving a reduced loss of transverse magnetization during the echo time.

Later in diastole the blood shows less signal than the surrounding cardiac muscle (Fig. 4*C* and *D* and last few frames of Figs 2 and 3). This may reflect turbulent flow of the blood entering the ventricle causing dephasing of spins within the echo time. For both the WKY and SHR in Fig. 2, the last few frames during diastole show dark blood

moving from the base to the apex of the left ventricle and displacing the brighter blood. The heart rate of the WKY used for the images shown in Fig. 2*A* (331 ± 3 beats min^{-1}) was a little higher than for the SHR used for the images shown in Fig. 2*B* (287 ± 7 beats min^{-1}). Consequently the dark blood which refilled the ventricles in diastole appeared slightly earlier in the image time series shown in Fig. 2*A* than that shown in Fig. 2*B*. The blood contrast, in general, showed no difference between the WKY and SHR, allowing the same analysis procedures to be applied to both strains.

The blood in the aorta provided little signal during systole, particularly between 34 and 86 ms in the WKY example (Fig. 2*A*). This may reflect rapid signal dephasing from fluid turbulence or high shear rates in a laminar flow regime when the blood is flowing within the imaged slice. During

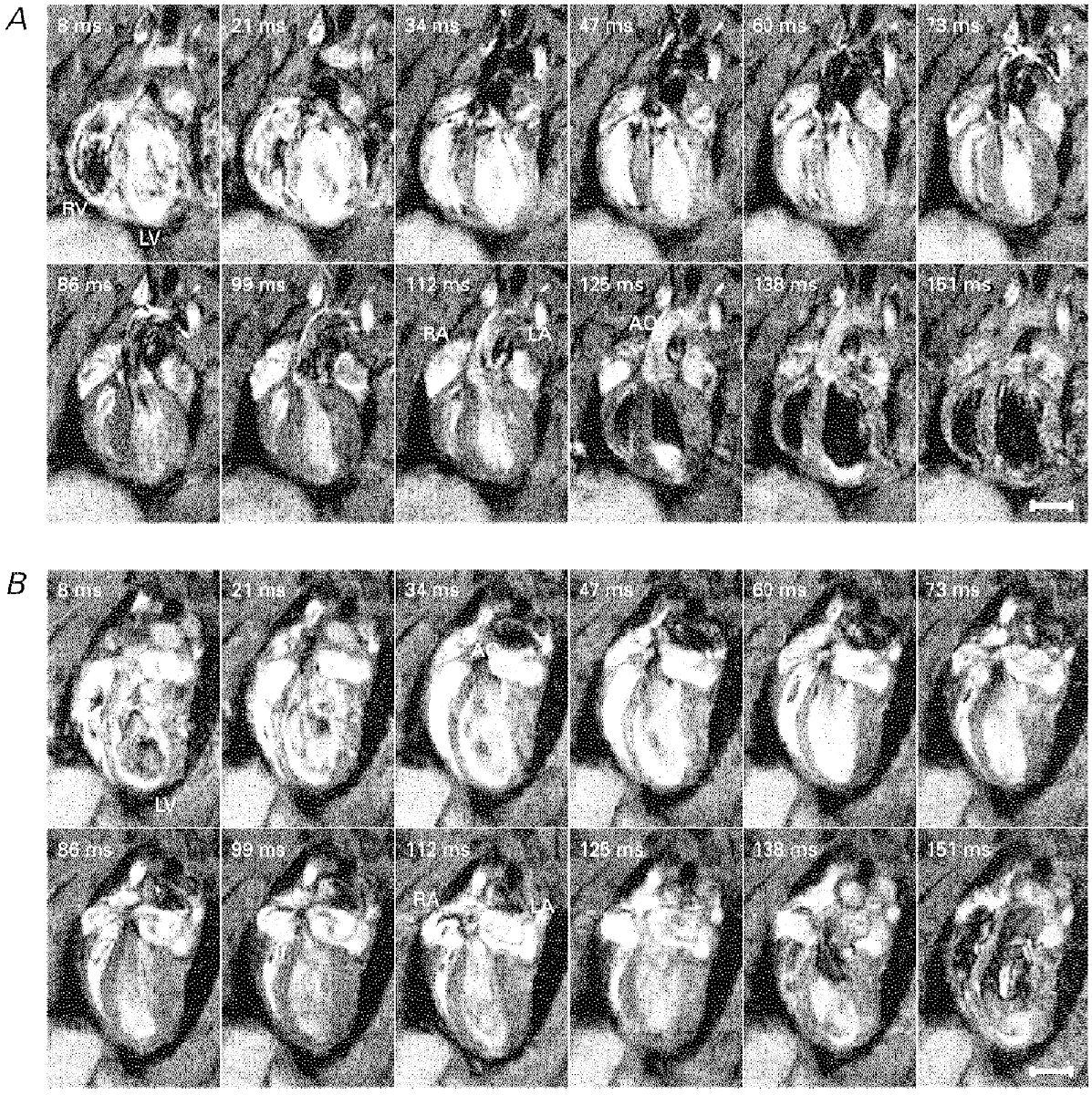

Figure 2. Longitudinal cardiac sections

A series of typical longitudinal sections taken parallel to the principal cardiac axis at one spatial slice obtained from a normal male WKY weighing 300 g and aged 12 weeks (*A*) and from a male SHR weighing 319 g and aged 12 weeks (*B*). The intrinsic heart rates of these rats were 331 ± 3 and 287 ± 7 beats min^{-1}, respectively. Each image is the average of two signals obtained at corresponding points in the cardiac cycle following the R wave. The time indicated in the upper left-hand corner of each panel is the delay after the trigger, taken from the R wave, at which each signal was acquired. The left and right ventricles (LV and RV), atria (LA and RA) and the aorta (AO) are labelled. The nominal in-plane resolutions (pixel sizes) were 350 and 390 μm for the WKY and SHR, respectively, and slice thicknesses were 1·12 mm for both animals. For display, the images have been zero-padded from a matrix of 128 to 256 pixels square. The effective repeat time was approximately 400 ms. The scale bars indicate 5 mm.

diastole, slower moving blood appeared considerably brighter. The atria displayed particularly high signal intensity (inflow brightening) at around 112 ms after the R wave trigger (Fig. 2*A* and *B*), just after end-systole.

Left ventricular contraction largely involved thickening of the wall and a reduction in ventricular radius in the transverse plane in both the WKY and SHR, particularly around the widest region of the left ventricle (Fig. 2). Systole also produced a comparatively smaller but significant, longitudinal shortening of the left ventricle (Fig. 8). Such motion is thought to be important in human cardiac function (Karwatowski *et al.* 1994*a*,*b*). The LV wall was considerably thinner near the apex in both the WKY and SHR (Fig. 2).

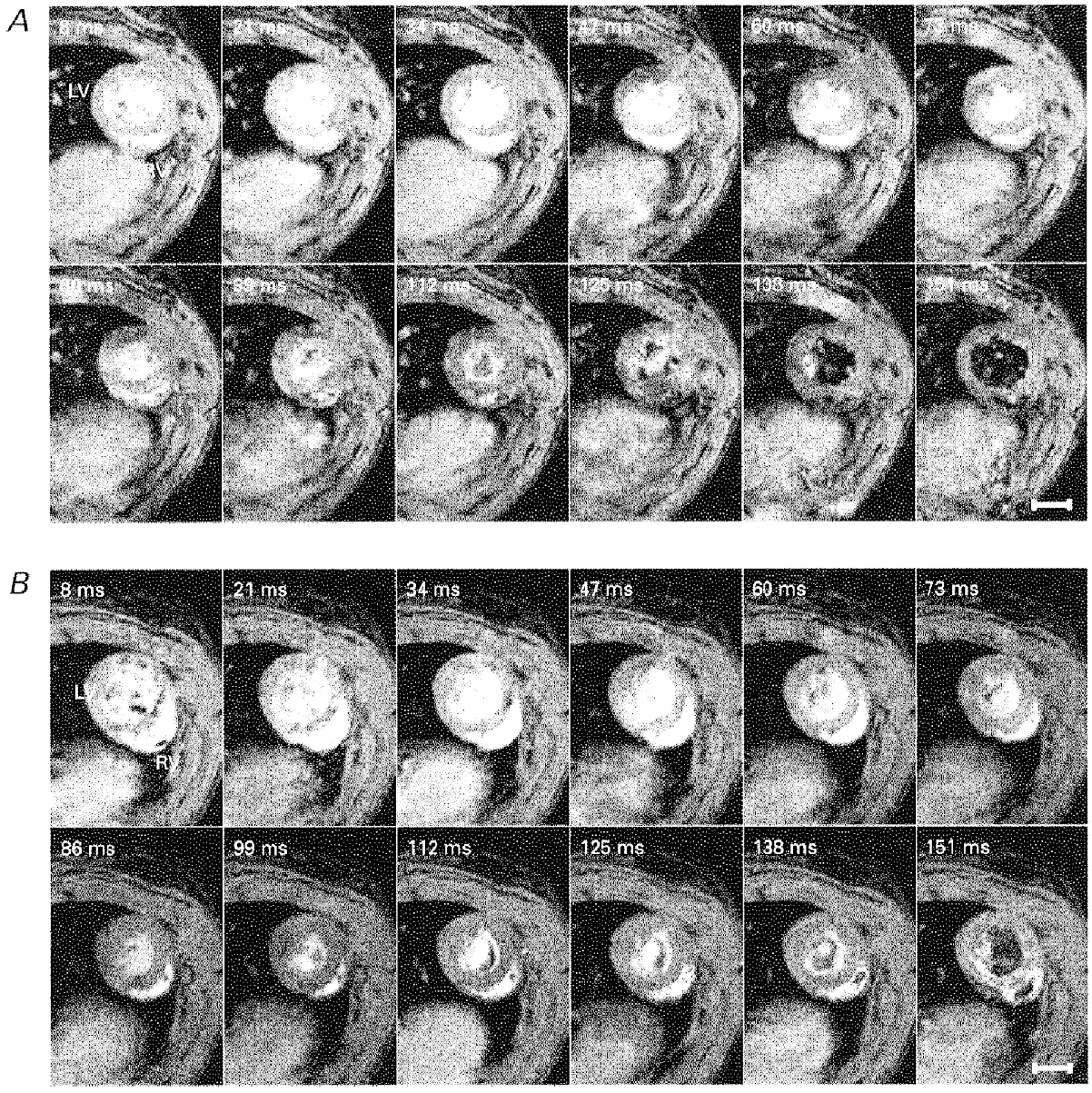

Figure 3. Transverse cardiac sections

A series of typical transverse sections taken at right angles to the principal cardiac axis at one spatial slice obtained from a normal male WKY weighing 309 g and aged 12 weeks (*A*) and a male SHR weighing 319 g and aged 12 weeks (*B*). Intrinsic heart rates were 295 ± 4 beats min^{-1} for the WKY rat and 287 ± 7 beats min^{-1} for the SHR. Each image is the average of two signals obtained at corresponding points in the cardiac cycle following the R wave. The time indicated in the upper left-hand corner of each panel is the delay after the trigger, taken from the R wave, at which the signal was acquired. LV and RV indicate the left and right ventricles, respectively. The nominal in-plane resolutions for the WKY and SHR were, respectively, 350 and 390 μm and slice thicknesses were 1·44 and 1·37 mm. For display, the images have been zero-padded from a matrix of 128 to 256 pixels square. The effective repeat time was approximately 400 ms. The scale bars indicate 5 mm.

Figure 3 shows the right ventricle as a crescent-shaped appendage attached to the left ventricle, also showing similar blood–muscle contrast. The consistent position of the right ventricle throughout the cardiac cycle indicates that there is little cardiac rotation during contraction, in contrast to the complex cardiac motion seen in humans (Azhari *et al.* 1992). Similarly, the longitudinal sections of Fig. 2 show no obvious rotation of the heart within the longitudinal plane and consequently little motion of the longitudinal axis of the heart in the WKY and SHR. These observations are important for simplifying subsequent quantitative geometrical analysis of the left ventricle.

In the transverse plane in both the WKY and SHR, the left ventricle shows circular symmetry of the epi- and endocardial borders at most points during the cardiac cycle (Fig. 3). Both the endocardial and epicardial LV surfaces were approximately elliptical in shape in longitudinal section (Fig. 2) in both the WKY and SHR strains. These symmetry properties are used below as a basis for geometrical descriptions of the left ventricle. Qualitative inspection of the images (Figs 2 and 3) revealed little difference in the anatomy of the WKY and SHR left ventricles (Fig. 3*A* and *B*), justifying our use of the same analytical techniques on both strains in order to compare their major functional cardiac parameters (see below).

The image sections are geometrically consistent

Two precautions, one experimental and the other analytical, confirmed that the heart remained in a stable physiological state throughout the duration of the imaging sessions. Typically it took about 20 min to acquire a complete multi-slice image data set for the left ventricle, over many time

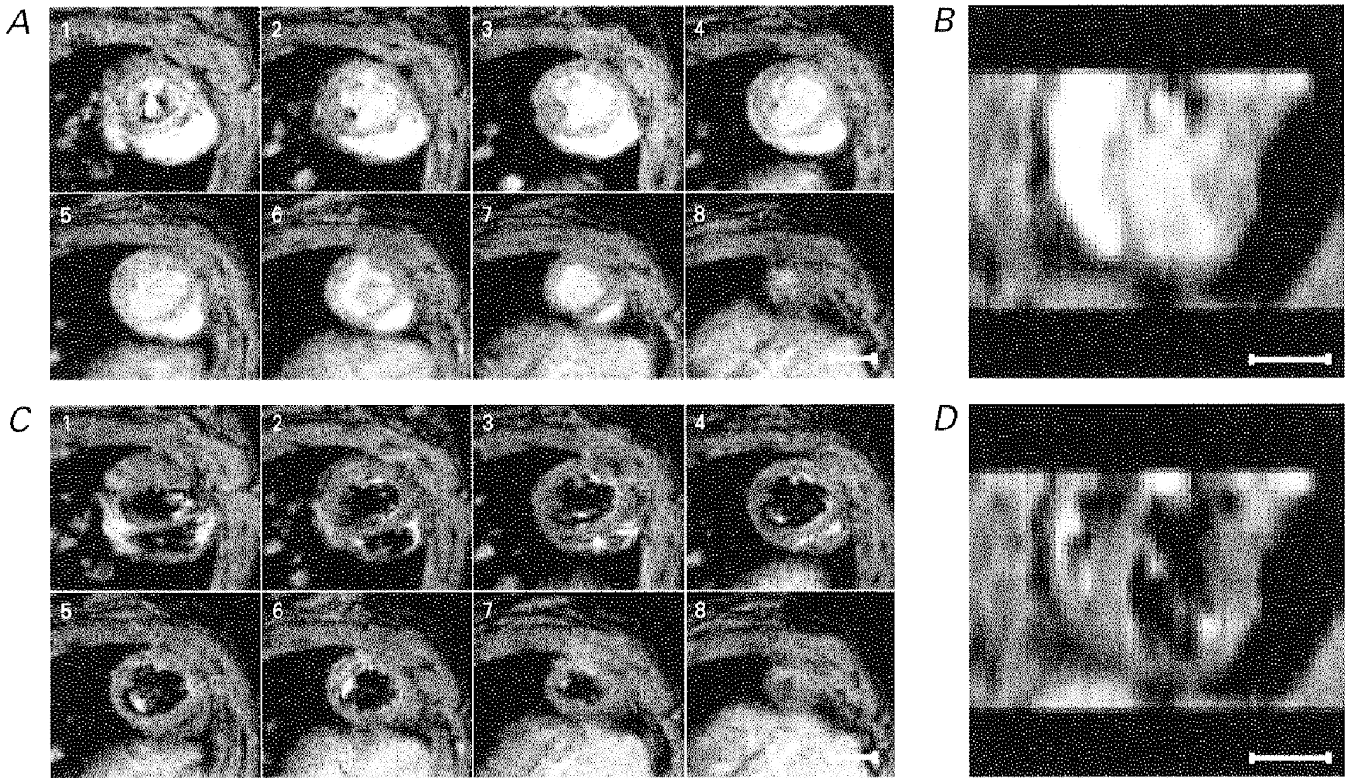

Figure 4. Contiguous cardiac sections

A and *C* show a series of typical contiguous transverse cardiac sections taken through the principal cardiac axis at successive levels from base to apex of the heart. Image acquisition was synchronized to the R wave of the cardiac cycle. *A* shows the images taken 34 ms after the R wave trigger, during systole, and *C* shows the corresponding slices at 138 ms after the trigger, during diastole. For display purposes only 8 of the possible 12 slices of each data set are shown: frame 1 was taken near the aortic outflow and frame 8 at the apex of the heart. The corresponding slices at two different time points in the cardiac cycle indicate the different contrast regimes from the imaging protocol, clearly demarcating the ventricular wall and the ventricular lumen. These images were obtained from a normal male WKY weighing 239 g. The intrinsic heart rate of this rat was 304 ± 7 beats min^{-1}. Each image is the average of two signals obtained at corresponding points in the cardiac cycle following the R wave. The slice thickness was 1·32 mm with a nominal in-plane resolution of 390 μm. *B* and *D* show these same data reconstructed into longitudinal sections by stacking the slices of the transverse multislice data sets on top of one another and cutting the resulting data set squarely through the left and right ventricles, which can be seen clearly. Comparison with Fig. 2 confirms the geometrical consistency of the transverse cardiac slices used for detailed analysis. The scale bars indicate 5 mm.

points during the cardiac cycle and including signal averaging. Furthermore, establishing self-consistency of the images enabled events in the cardiac cycle to be identified and the cardiac function to be analysed with confidence.

Firstly, the multislice data sets were bracketted at the start and finish of the imaging sessions by acquiring spatially equivalent data sets to confirm that the animal had not moved within the bore of the magnet. Secondly, the multislice data sets were examined as a whole to confirm that the contiguous image slices formed an internally consistent data set that could be constructed into a three-dimensional representation of the heart, amenable to quantitative analysis. Figure 4 demonstrates such an analysis during systole (Fig. 4*A* and *B*) and diastole (Fig. 4*C* and *D*). Figure 4*A* and *C* illustrates transverse cardiac sections perpendicular to the principal cardiac axis at successive levels from the aortic outflow (frame 1) to the apex (frame 8). The transverse slices assumed equivalent positions in each frame. Figure 4*B* and *D* shows the results of stacking the transverse image sections to yield reconstructed longitudinal sections. These display smooth LV boundaries that closely resemble the equivalent directly acquired sections (Fig. 2).

Comparison of LV myocardial volumes derived from the transverse (Fig. 3) and longitudinal (Fig. 2) cardiac sections revealed a linear correlation (Pearson's correlation coefficient $r = 0{\cdot}93$), with a least squares linear fit yielding $y = 0{\cdot}79\ (\pm\ 0{\cdot}12)\,x + 85\ (\pm\ 64)\ \mu$l (68·3% confidence interval). The linear relationship confirms the repeatability and consistency of volume measurements made using differently orientated imaging planes. Systematic differences may result from differences in the degree of LV truncation employed along the long cardiac axis. Furthermore, the effects of finite slice thickness and partially filled image voxels (partial volume effects) may be consistently larger for the longitudinal cardiac sections, since there were fewer of these sections than the transverse sections covering the ventricle.

Comparison of LV borders defined by two independent observers verified that inter-observer variability was small. A least squares linear regression of the image cross-sectional areas produced from the two observers gave $y = 1{\cdot}01\ (\pm\ 0{\cdot}01)x - 1{\cdot}3\ (\pm\ 0{\cdot}4)$ mm^2 (68·3% confidence intervals) and Pearson's correlation coefficient $r = 0{\cdot}99$.

Consistency with histological results

The measurements from the living rat heart obtained using MRI agreed with independent histological measurements. MRI derived LV muscle volumes were calculated by subtracting empirical LV endocardial volumes from the epicardial volumes. Figure 5*A* plots the LV myocardial volumes, given as the mean values established from all the time points imaged during the cardiac cycle, against the directly determined *ex vivo* LV muscle mass. It confirms a linear correlation between the muscle volumes determined by MRI and the directly determined muscle mass ($r = 0{\cdot}81$). Figure 5*A* suggests a density of LV muscle of $0{\cdot}94\ (\pm\ 0{\cdot}18)$ g cm^{-3} from the slope of the linear regression ($y = 0{\cdot}94\ (\pm\ 0{\cdot}18)x + 0{\cdot}20\ (\pm\ 0{\cdot}10)$ g), consistent with the value of 1·05 g cm^{-3} reported previously (Manning *et al.* 1990), with any differences in muscle density being the systematic result of tissue fixation. The latter caused tissue shrinkage and a consequent reduction in tissue mass in both the WKY and SHR. Myocardial densities were similar in both the SHR and WKY groups.

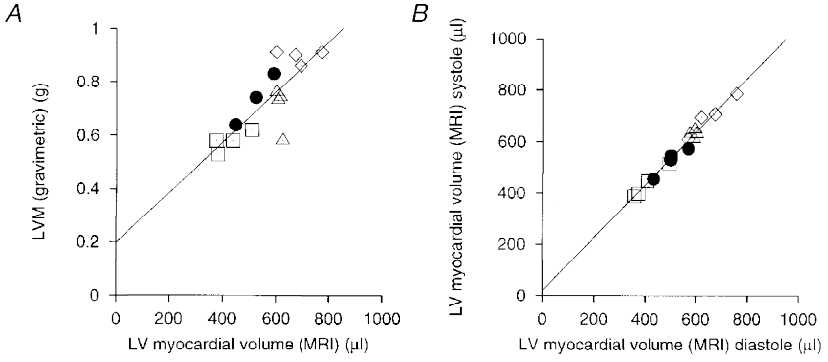

Figure 5. Left ventricular muscle volumes

A, correlation of LV myocardial volume determined by MRI and post-mortem LV mass ($r = 0{\cdot}81$). The line shows the least squares fit for these data ($y = 0{\cdot}94\ (\pm\ 0{\cdot}18)x + 0{\cdot}20\ (\pm 0{\cdot}10)$ g), giving an estimated myocardial density of $0{\cdot}94\ (\pm\ 0{\cdot}18)$ g cm^{-3}. *B*, correlation of the MRI determined LV myocardial volume towards end-systole and end-diastole ($r = 0{\cdot}99$). The LV muscle volume was determined at each time point (typically 12 of them) for each rat. The volume at each of three time points near end-systole and diastole was used to give a mean LV muscle volume at these two points in the cardiac cycle; these are the volumes correlated here. A linear least squares fit gave $y = 1{\cdot}03\ (\pm\ 0{\cdot}04)x + 20\ (\pm\ 21)\ \mu$l, indicating a close agreement between LV muscle volume determined, at these two points in the cardiac cycle, from the MR images. 68·3% confidence intervals are given in parentheses. □, 8 week WKY; ●, 12 week WKY; △, 8 week SHR; ◇, 12 week SHR.

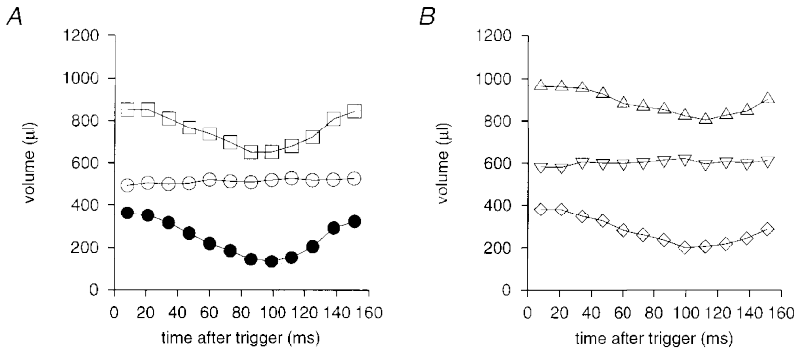

Figure 6. Time series of left ventricular volume

Endo-, epi- and myocardial LV volumes for one typical WKY rat (*A*; □, epicardial; ○, myocardial; ●, endocardial) and one typical SHR (*B*; △, epicardial; ▽, myocardial; ◇, endocardial) plotted against time after the R wave trigger, measured from transverse MR sections. Heart rates were 293 ± 3 beats min^{-1} for the SHR and 304 ± 7 beats min^{-1} for the WKY. The SHR and WKY rats used for measuring these volumes had very similar body weights (241 and 239 g, respectively). The LV myocardial volume was greater in the SHR and its ejection fraction was reduced, as indicated by the raised end-systolic volume compared with the WKY. This is consistent with the overall parameters for each group of animals specified in Table 1.

The scatter in Fig. 5*A* probably reflects variations in dissection of the left ventricle from the rest of the heart. This is likely to be a more significant source of uncertainty than that derived from the MRI volume measurements. The latter would particularly concern the extent of left ventricle defined in the MRI data set. These uncertainties would account for the non-zero y-intercept of Fig. 5*A*.

Conservation of myocardial volume throughout the cardiac cycle

Figure 5*B* compares the LV muscle volume at end-systole and end-diastole from the transverse cardiac MR sections. It confirms a close correlation ($r = 0{\cdot}99$) between the two time points with a least squares linear fit of $y = 1{\cdot}03\ (\pm\ 0{\cdot}04)x + 20\ (\pm\ 21)\ \mu l$ (68·3% confidence interval). The small residual difference may reflect differences in the definition of borders when the heart changes its shape during systole, for example in the additional convolution of the endocardial surface. However, these findings confirm the consistency of the protocol for defining the epi- and endocardial borders and additionally indicate its potential use in assessing the development of ventricular hypertrophy and LV function.

Left ventricular parameters

The systolic blood pressure of the animals soon after the anaesthesia but before the actual MR examination confirmed hypertension in the SHR in both age groups examined compared with the controls. Table 1 displays systolic blood pressure values for both age groups of the two animal strains. Figure 6 displays empirically derived LV epicardial, endocardial and luminal volumes for a typical WKY and SHR of similar body weight, throughout the cardiac cycle, with 13 ms time resolution. It confirms a conservation of LV myocardial volume throughout the cardiac cycle and demonstrates the similar shapes of the volume–time curves in the WKY and SHR, with an accelerating contraction of the ventricle towards the beginning of systole. Figure 6 suggests that the SHR may experience slower refilling during diastole, at a similar heart rate; whether this is a feature of cardiac function in the SHR in general needs further study. In Fig. 6*B* the raised end-systolic endocardial volume of the left ventricle is consistent with the results displayed in Table 1.

The end-diastolic volume (EDV), when the luminal volume of the left ventricle was maximal, was obtained from the

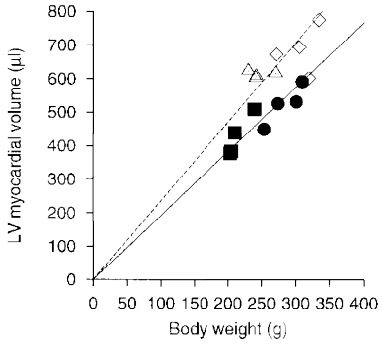

Figure 7. Left ventricular myocardial volume *versus* body weight

An intercept through the origin is assumed and a linear fit produces LVMV/BW ratios of 1·92 ± 0·05 and 2·36 ± 0·09 $\mu l\ g^{-1}$ (68·3% confidence intervals) for combined age groups of WKY and SHR, respectively (Table 1). ■, 8 week WKY; ●, 12 week WKY; △, 8 week SHR; ◇, 12 week SHR.

images acquired typically 8–20 ms after the trigger pulse from the R wave of the ECG. The end-systolic volume (ESV) was taken as the minimum luminal volume of the left ventricle. The ejection fraction (EF) is the proportion of blood, at end-diastole, which was expelled from the left ventricle during systole and was calculated using the formula:

$$EF = (EDV - ESV)/EDV. \quad (1)$$

The control WKY group and the SHR group had comparable body weights (BW) with no significant difference between the two groups. Both groups showed an increase in body weight between 8 and 12 weeks of age and also a corresponding increase in the total LV myocardial volume (Table 1 and Fig. 7). However, the SHR group as a whole showed a 36% larger LV myocardial volume than the control WKY group (Table 1 and Fig. 7). When this was normalized with respect to the body weight of the animals the SHR group showed a significantly larger (23%) LV myocardial volume-to-body weight ratio (LVMV/BW), given by the gradient of the fitted lines constrained to pass through the origin of the plot in Fig. 7. This indicates development of LV hypertrophy in the SHR relative to WKY. The WKY and SHR groups both showed a smaller LVMV/BW ratio for the 12 week groups than the 8 week groups (Table 1). Laurent *et al.* (1995) have previously used an allometric formula for normalizing myocardial masses (and therefore volumes) to quantify LV hypertrophy (LVH), given by (left ventricular mass)/$(BW)^{0.7}$. The present study adopts a simple linear normalization with respect to body weight, since the narrow range of body weights shown here did not necessitate such a non-linear regression relationship. Furthermore, the WKY and SHR had approximately the same range of body weights in this study, making a power law relationship unnecessary for showing the relative differences in LV myocardial volume. The LV myocardial volume could be converted to muscle mass by simply assuming a uniform specific gravity of 1·05 g cm^{-3} (Manning *et al.* 1990).

End-diastolic and end-systolic luminal volumes of the left ventricle increased with age in both groups of rats (Table 1). There was relatively little difference in end-diastolic volume between the WKY and SHR groups. However, end-systolic volume was significantly larger in the SHR group, producing a lower ejection fraction and hence significantly poorer emptying of the left ventricle in the SHR group compared with the WKY group. This is consistent with the findings of Laurent *et al.* (1995).

The cardiac parameters such as ejection fraction and the LVMV/BW ratio appeared to change little in the SHR group between the two age groups (Table 1), relative to the controls. This may indicate that the SHR is a rather stable model with respect to LV structure and function, over the observed age range.

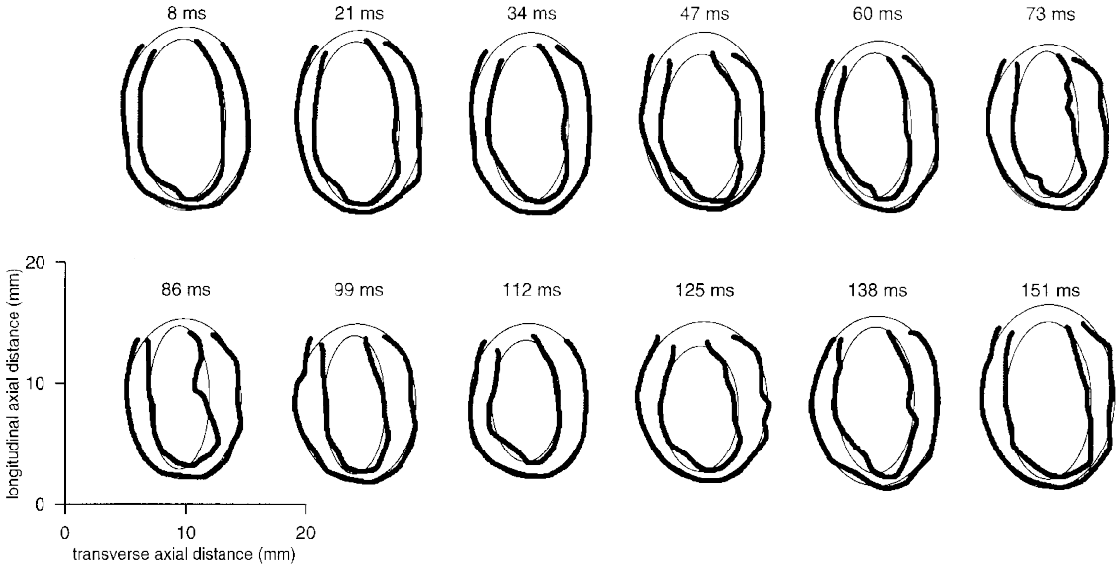

Figure 8. Left ventricular borders and fitted ellipses from longitudinal image sections

A series of epi- and endocardial borders (thick lines) and corresponding fitted ellipses (thin lines), for a single longitudinal cardiac slice, of a similar type to those shown in Fig. 2, through the widest point across the left ventricle. Borders are shown for all 12 cardiac time points imaged during the cardiac cycle in an 8-week-old male WKY (body weight 203 g, heart rate 353 ± 5 beats min^{-1}). The time indicated above each panel is the delay after the trigger, taken from the R wave of the ECG, at which the image corresponding to the borders was acquired. The interactively defined epicardial borders lie outside the endocardial borders. The incompleteness of the borders at one end of the ventricle reflects the presence of the aortic outflow. Contraction of the ventricle and corresponding thickening of the myocardial wall can be seen during systole (8–99 ms) after the trigger, followed by an expansion of the ventricle during diastole.

Left ventricular geometry approximated using a single longitudinal cardiac section

We next developed a simple geometrical model of the left ventricle which aimed to describe its function using a considerably reduced set of imaging planes (Underwood *et al.* 1988; Cranney *et al.* 1990). Such a model is potentially valuable for reducing experimental imaging time in future serial animal studies. Figure 2 demonstrates an elliptical shape of the epi- and endocardial borders of the left ventricle in both the WKY and SHR in longitudinal sections through the widest region of the left ventricle. Figure 8 displays interactively defined epi- and endocardial LV borders for one WKY (thick lines), further suggesting the elliptical shape of these borders. Figure 3 demonstrated that the epi- and endocardial LV borders were circular in transverse section. Taken together, these findings led us to describe the LV volumes using ellipses rotated about the principal cardiac axis with myocardial volumes estimated by subtracting the epicardial volume from the endocardial.

A least squares minimization procedure fitted a two-dimensional ellipse (Fig. 8), given by:

$$R^2 = (x - x_0)^2 + a^2(z - z_0)^2, \quad (2)$$

to the longitudinal epi- and endocardial borders at each imaged time point independently, where x is the co-ordinate in the transverse direction, z is the co-ordinate along the longitudinal (principal) axis of the heart, (x_0, z_0) is the centre of the ellipse, $2R$ is the minor axis length and $2R/a$ is the length of the major axis. The least squares fitting searched the parameter space (R, a, x_0, z_0) to minimize the total residual square distance of the points on the LV border from the ellipse.

Figure 9*A* shows the resulting predictions of the endo-, epi- and myocardial LV volumes throughout the cardiac cycle, for one WKY, comparing them with empirically derived volumes from the multislice transverse images. The modelled and empirical endocardial volumes closely agreed throughout the cardiac cycle.

Figure 9*B* compares the end-diastolic and end-systolic endocardial LV volumes from this simple model with the empirical analysis. There was no significant difference in the relationship of the endocardial LV volumes between the WKY and SHR groups and there was a linear correlation between the model and empirical volumes ($r = 0{\cdot}95$). Table 2 confirms good numerical agreement between the modelled and empirical end-diastolic volumes, end-systolic volumes and ejection fractions derived from the endocardial LV borders for the WKY and SHR groups. The modelled parameters reflect the relatively raised end-systolic volume and associated reduced ejection fraction in the SHR group compared with the WKY group.

The elliptical model consistently overestimated the epicardial volumes (Fig. 9*A*) and consequently the model agrees less well (Table 2) with the empirically derived LV myocardial volume. As a result there was little correlation between the modelled and empirical LV myocardial volume normalized with respect to body weight (a measure of LV hypertrophy). This may result from a differing distribution of muscle in the LV wall in the WKY and SHR groups. The

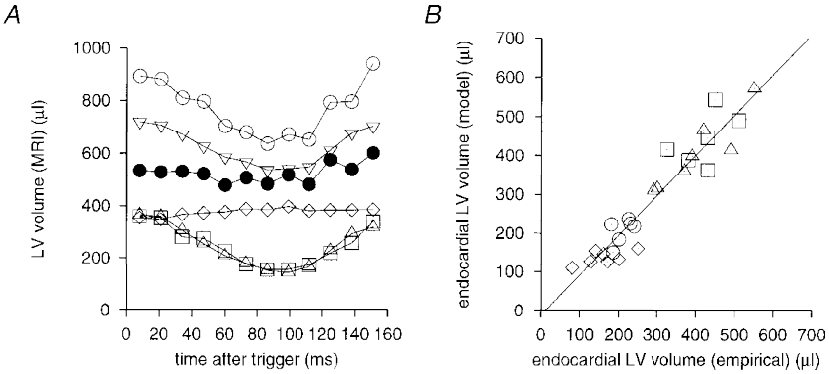

Figure 9. Comparison of modelled and empirical left ventricular volume

A, endo-, epi- and myocardial LV volumes plotted against time after the R wave trigger, both empirically derived from the multislice transverse images (△, endocardial; ▽, epicardial; ◇, myocardial) and derived from the single slice elliptical model (□, endocardial; ○, epicardial; ●, myocardial). The modelled data were extracted from the same animal as that displayed in Fig. 8. Modelled and empirical endocardial volumes are in close agreement throughout the cardiac cycle, while the epicardial and consequently the myocardial volumes are consistently overestimated by the elliptical model when compared with the empirical values. *B*, a comparison of the endocardial end-diastolic and end-systolic LV volumes from empirical analysis, using the multislice transverse cardiac images, and the single longitudinal slice elliptical model for both the WKY ($n = 7$; △, end-diastolic; ◇, end-systolic) and SHR ($n = 6$; □, end-diastolic; ○, end-systolic) groups. No significant difference in the relationship between these groups is evident. There is a linear correlation ($r = 0{\cdot}95$) with a line of best fit $y = 1{\cdot}03\ (\pm\ 0{\cdot}07)x - 11\ (\pm\ 22)\ \mu$l (63·8% confidence intervals).

Table 2. Comparison of modelled and empirical cardiac parameters

	WKY				SHR			
	Empirical		Model		Empirical		Model	
	Mean	S.E.M.	Mean	S.E.M.	Mean	S.E.M.	Mean	S.E.M.
LV myocardial volume by MRI (LVMV) (μl)	471	33	583	27	649	27	644	40
LVMV/BW (μl g^{-1})	1·89	0·04	2·36	0·07	2·36	0·11	2·33	0·07
End-diastolic volume (μl)	401	36	404	35	421	26	440	27
End-systolic volume (μl)	161	21	136	7	210	10	206	13
Ejection fraction	0·61	0·02	0·65	0·02	0·50	0·02	0·53	0·02

Major cardiac parameters for the WKY ($n = 7$) and SHR ($n = 6$) groups, derived from the empirical analysis of the transverse imaging sections covering the left ventricle, compared with those from the elliptical model based on one longitudinal slice. Values quoted are the means and S.E.M. values. LVMV/BW represents the LV muscle volume normalized with respect to body weight.

choice of a consistent single longitudinal slice to represent the whole ventricle may cause an overestimate of the total muscle in the WKY left ventricle if it is relatively thicker in the plane of the chosen slice; that possibility requires further analysis of local wall thickness. However, it is more likely that errors in LV myocardial volume estimation will result from the prediction in the model of the presence of cardiac muscle in the region of the aortic outflow (Fig. 8) in the left ventricle, when inspection of Fig. 2 shows that there is none.

DISCUSSION

MRI is a recent addition to the inventory of quantitative physiological measurement techniques, providing good soft tissue contrast and good anatomical and temporal image resolution. We examined two age groups of young adult WKY and SHR (8 and 12 weeks of age) by MRI to characterize cardiac changes in this model of hypertension in the relatively early stages of the disease. Two age groups were employed to probe development of the disease pathology. The SHR showed elevated systolic blood pressure compared with the WKY controls. Both strains of rat, WKY and SHR, presented similar body weights, allowing their cardiac function to be compared with confidence. The study showed differences in some morphological and functional parameters between the SHR and controls (Laurent *et al.* 1995), established from the anatomical MRI data.

MRI techniques were successfully developed to image the beating rat heart for full quantitative analysis, despite the challenges presented by the small size and rapid heart rate of a small mammal. Complete image coverage of the left ventricle by contiguous image sections in the anaesthetized rats was achieved using a short echo time (5 ms) multislice gradient-echo imaging sequence, in a manageable imaging time. The short echo time minimized motion artifacts and reduced signal loss from the blood pool during systole. Good time resolution (13 ms) between imaged time points of the cardiac cycle was achieved. RF probes were designed to maximize animal comfort, and a repeatable slice positioning protocol ensured acquisition of geometrically consistent and reproducible series of sections. The sections were acquired both parallel and perpendicular to the principal cardiac axis, beginning at end-diastole and continuing through most of the cardiac cycle. The transverse and longitudinal cardiac sections showed complementary features of the cardiac anatomy, including all four chambers, with good delineation of especially the epi- and endocardial borders of the left ventricle. They also illustrated the symmetry of the left ventricle.

Repeated acquisition of identical imaging planes at the start and end of each imaging session confirmed the physiological and positional stability of the animal during each imaging session. Comparison of images in orthogonal planes confirmed geometrical consistency of the image data sets. Such tests confirmed the suitability of data sets for quantitative analysis and modelling. Images were used to define the epi- and endocardial LV surfaces, enabling LV volumes to be established throughout the cardiac cycle. From these, major cardiac structural and functional parameters were derived in the two groups of age-matched normal WKY and SHR. The empirically determined LV myocardial volumes were verified against histologically determined myocardial mass and conservation of LV myocardial volume was confirmed.

The control WKY group and the SHR group had similar body weights, with no significant difference between the two groups, allowing direct comparison of cardiac parameters. Furthermore, within each strain, there was a significant increase in body weight between 8 and 12 weeks of age, the increase being similar for both strains. Both age groups of SHR showed a significantly increased ratio of LV myocardial volume to body weight, compared with the WKY controls,

indicating LV hypertrophy in the SHR. In addition, end-systolic volume was significantly larger in the two SHR age groups, giving a correspondingly poorer ejection fraction. These observations are consistent with the findings of Laurent *et al.* (1995). Comparison of these quantities between age groups showed no marked worsening of pathology between 8 and 12 weeks in the SHR compared with the controls. Therefore, the SHR appears to be a rather stable model with respect to LV structure and function, for the two age groups of animal used in this study. Future MRI studies with very young rats may be used to determine the relationship between the hypertension and very early changes in LV structure and function.

Finally a simple geometrical model of the left ventricle was developed, prompted by the symmetry of the left ventricle in our images. It used an elliptical figure to describe the LV shape from a single longitudinal section through the widest point of the left ventricle. The volumes generated by rotation of the two-dimensional ellipses were compared with empirically derived volumes from complete transverse cardiac multislice data sets. The model successfully reproduced functional parameters of the left ventricle including the end-diastolic volume, the end-systolic volume and ejection fraction in the WKY and SHR when compared with empirically derived volumes. Such a model is potentially important in allowing imaging time to be reduced, by employing a reduced set of imaging planes in future serial studies of cardiac function in rats.

Some recent MRI studies have examined functional parameters of the heart in small mammals (Manning *et al.* 1990; Rudin *et al.* 1991; Rose *et al.* 1994; Laurent *et al.* 1995; Rehwald *et al.* 1997; Franco *et al.* 1997; Lorenz *et al.* 1997; Slawson *et al.* 1997), and some of these have employed spin-echo imaging (Manning *et al.* 1990; Rudin *et al.* 1991; Laurent *et al.* 1995). Unlike the present study, these studies did not generally combine the evaluation in both normal (WKY) and hypertensive (SHR) rats of LV volume at high time resolution throughout the cardiac cycle with the application of short echo time gradient-echo MRI using multiple image planes oriented using a robust slice positioning protocol. Some previous studies concentrated on imaging only at end-systole and end-diastole (Laurent *et al.* 1995) while in the present study many frames were acquired throughout the cardiac cycle, allowing contraction and relaxation of the left ventricle to be closely examined over time. Furthermore, unlike these previous studies, we have evaluated a technique for examining cardiac function with reduced imaging and analysis time, by careful choice of image sections.

We have successfully used our MRI protocol with good temporal resolution to characterize cardiac function in normal and hypertensive rats. Future analysis of such image data sets may reveal dynamic parameters of the left ventricle such as the rate of contraction and refilling ($\mathrm{d}V/\mathrm{d}t$). This may then contribute to a comprehensive physical modelling of stress, pressure and flow in the left ventricle. In addition, major cardiac parameters for the right ventricle may be established to examine the low pressure circulation in normal and spontaneously hypertensive rats. The imaging and analysis techniques which we have described have the potential to be applied in many different animal models of human cardiovascular disease.

Axel, L. & Dougherty, L. (1989). Heart wall motion: improved method of spatial modulation of magnetisation for MR imaging. *Radiology* **172**, 349–350.

Azhari, H., Buchalter, M., Sideman, S., Shapiro, E. & Beyar, R. (1992). A conical model to describe the nonuniformity of the left ventricular twisting motion. *Annals of Biomedical Engineering* **20**, 149–165.

Baldy, C., Douek, P., Croisille, P., Magnin, I. E., Revel, D. & Amiel, M. (1994). Automated myocardial edge detection from breath-hold cine-MR images: evaluation of left ventricular volumes and mass. *Magnetic Resonance Imaging* **12**, 589–598.

Ballon, D., Graham, M. C., Midownik, S. & Koutcher, J. A. (1990). A 64 MHz half-birdcage resonator for clinical imaging. *Journal of Magnetic Resonance* **90**, 131–140.

Beall, P. T., Amtey, S. R. & Kasturi, S. R. (1984). *NMR Data Handbook for Biomedical Applications*. Pergamon Press, New York.

Bishop, S. P. (1980). Cardiovascular research. In *The Laboratory Rat*, vol. 2, pp. 162–172. Academic Press Inc., New York.

Carpenter, T. A., Hall, L. D. & Jezzard, P. (1989). Proton magnetic resonance imaging of solid polymers using instrumentation designed for the liquid state. *Journal of Magnetic Resonance* **84**, 383–387.

Cranney, G. B., Lotan, C. S., Dean, L., Baxley, W., Bouchard, A. & Pohost, G. M. (1990). Left ventricular volume measurement using cardiac axis nuclear magnetic resonance imaging, validation by calibrated ventricular angiography. *Circulation* **82**, 154–163.

Crooks, L. E., Barker, B., Chang, H., Feinburg, D., Hoenninger, J. C., Watts, J. C., Mitsuaki, A., Kaufman, L., Sheldon, P. E., Botvinick, E. & Higgins, C. B. (1984). Magnetic resonance imaging strategies for heart studies. *Radiology* **153**, 459–465.

Crowley, J. J., Huang, C. L.-H., Gates, A. R. C., Basu, A., Shapiro, L. M., Carpenter, T. A. & Hall, L. D. (1997). A quantitative description of dynamic left ventricular geometry in anaesthetized rats using magnetic resonance imaging. *Experimental Physiology* **82**, 887–904.

Decrespigny, A. J. S., Carpenter, T. A. & Hall, L. D. (1991). Cardiac tagging in the rat using a DANTE sequence. *Magnetic Resonance in Medicine* **21**, 151–156.

Forbat, S. M., Karwatowski, S. P., Gatehouse, P. D., Firmin, D. N., Longmore, D. B. & Underwood, S. R. (1994). Rapid measurement of left ventricular mass by spin echo magnetic resonance imaging. *British Journal of Radiology* **67**, 86–90.

Franco, F., Dubois, S., Sander, M., Sholet, R. V. & Peshock, R. M. (1997). Magnetic resonance imaging accurately estimates left ventricular mass in a transgenic mouse model of hypertrophy. In *Proceedings of the International Society for Magnetic Resonance in Medicine* (*5th Scientific Meeting and Exhibition*), p. 887. International Society for Magnetic Resonance in Medicine, Berkeley, CA, USA.

Greenbaum, R. A., Ho, S. Y., Gibson, D. G., Becker, A. E. & Anderson, R. H. (1981). Left ventricular fibre architecture in man. *British Heart Journal* **45**, 248–263.

Karwatowski, S. P., Mohiaddin, R. H., Yang, G. Z., Firmin, D. N., Sutton, M. S. & Underwood, S. R. (1994*a*). Regional myocardial velocity imaged by magnetic resonance in patients with ischaemic heart disease. *British Heart Journal* **72**, 332–338.

Karwatowski, S. P., Mohiaddin, R., Yang, G. Z., Firmin, D. N., Sutton, M. S., Underwood, S. R. & Longmore, D. B. (1994*b*). Assessment of regional left ventricular long-axis motion with MR velocity mapping in healthy subjects. *Journal of Magnetic Resonance Imaging* **4**, 151–155.

Laurent, D., Allegrini, P. R. & Zierhut, W. (1995). Different left ventricular remodelling and function in two models of pressure overload as assessed *in vivo* by magnetic resonance imaging. *Journal of Hypertension* **13**, 693–700.

Longmore, D. B., Bland, C., Burman, E. D., Denison, D. M., Firmin, D. N., Fox, K. M., Hounsfield, G. N., Klipstein, R. H., McNeilly, A. M., Poole-Wilson, P. A., Rees, R. S. O., Underwood, S. R. & Watanabe, M. (1985*a*). Clinical measurement of ventricular dimensions and stroke volume using magnetic resonance. *British Heart Journal* **53**, 674–675.

Longmore, D. B., Underwood, S. R., Hounsfield, G. N., Bland, C., Poole-Wilson, P. A., Denison, D., Klipstein, R. H., Firmin, D. N., Watanabe, M., Fox, K., Rees, R. S. O. & Burman, E. D. (1985*b*). Dimensional accuracy of magnetic resonance in studies of the heart. *Lancet* **i**, 1360–1362.

Lorenz, C. H., Henson, R. E., Creemers, M., Fischer, S. E. & Wickline, S. A. (1997). Regional ventricular function can be quantified in the rat and mouse with a 1.5T whole-body MR scanner. In *Proceedings of the International Society for Magnetic Resonance in Medicine* (*5th Scientific Meeting and Exhibition*), p. 884. International Society for Magnetic Resonance in Medicine, Berkeley, CA, USA.

Manning, W. J., Wei, J. Y., Fossel, E. T. & Burstein, D. (1990). Measurement of left ventricular mass in rats using electrocardiogram-gated magnetic resonance imaging. *American Journal of Physiology* **258**, H1181–1186.

Mohiaddin, R. H. & Longmore, D. B. (1993). Functional aspects of cardiovascular nuclear magnetic resonance imaging. Techniques and application. *Circulation* **88**, 264–281.

Pettigrew, R. I. (1989). Dynamic cardiac MR imaging, techniques and applications. *Radiologic Clinics of North America* **27**, 1183–1203.

Pope, J. M. & Yao, S. (1993). Quantitative NMR imaging of flow. *Concepts in Magnetic Resonance* **5**, 281–302.

Rehr, R. B., Malloy, C. R., Filipchuk, N. G. & Peshock, R. M. (1985). Left ventricular volumes measured by MR imaging. *Radiology* **156**, 717–719.

Rehwald, W. G., Reeder, S. B., McVeigh, E. R. & Judd, R. M. (1997). Techniques for high-speed cardiac magnetic resonance imaging in rats and rabbits. *Magnetic Resonance in Medicine* **37**, 124–130.

Rose, S. E., Wilson, S. J., Zelaya, F. O., Crozier, S. & Doddrell, D. M. (1994). High resolution high field rodent cardiac imaging with flow enhancement suppression. *Magnetic Resonance Imaging* **12**, 1183–1190.

Rudin, M., Pedersen, B., Umemura, K. & Zierhut, W. (1991). Determination of rat heart morphology and function *in vivo* in two models of cardiac hypertrophy by means of magnetic resonance imaging. *Basic Research in Cardiology* **86**, 165–174.

Schnittger, I., Fitzgerald, P. J., Daughters, G. T., Ingels, N. B., Kantrowitz, N. E., Schwarzkopf, A., Mead, C. W. & Popp, R. L. (1982). Limitations of comparing left ventricular volumes by two dimensional echocardiography, myocardial markers and cineangiography. *American Journal of Cardiology* **50**, 512–519.

Sechtem, U., Pflugfelder, P. W., Gould, R. G., Cassidy, M. M. & Higgins, C. B. (1987). Measurement of right and left ventricular volumes in healthy individuals with cine MR imaging. *Radiology* **163**, 697–702.

Semelka, R. C., Tomei, E., Wagner, S., Mayo, J., Kondo, C., Suzuki, J.-I., Caputo, G. R. & Higgins, C. B. (1990). Normal left ventricular dimensions and function: interstudy reproducibility of measurements with cine MR imaging. *Radiology* **174**, 763–768.

Sibson, N. R., Burdett, N. G., Gates, A. R. C., Carpenter, T. A. & Hall, L. D. (1993). Physiological monitoring during magnetic resonance imaging of the anaesthetized rat. *Journal of Physiology* **459**, 307*P*.

Slawson, S. E., Roman, B. R. & Koretsky, A. P. (1997). Cardiac MRI of the normal and hypertrophied mouse heart. In *Proceedings of the International Society for Magnetic Resonance in Medicine* (*5th Scientific Meeting and Exhibition*), p. 887. International Society for Magnetic Resonance in Medicine, Berkeley, CA, USA.

Soldo, S. J., Norris, S. L., Gober, J. R., Haywood, L. J., Colletti, P. M. & Terk, M. (1994). MRI-derived ventricular volume curves for the assessment of left ventricular function. *Magnetic Resonance Imaging* **12**, 711–717.

Underwood, S. R., Gill, C. W. R., Firmin, D. N., Klipstein, R. H., Mohiaddin, R. H., Rees, R. S. O. & Longmore, D. B. (1988). Left ventricular volume measured rapidly by oblique magnetic resonance imaging. *British Heart Journal* **60**, 188–195.

Underwood, S. R., Longmore, D. B., Klipstein, R. H., Firmin, D. N., Watanabe, M., McNeilly, A. M., Burman, E. D., Denison, D., Fox, K., Hounsfield, G. N., Poole-Wilson, P. & Rees, R. S. O. (1985). Clinical validation of left and right ventricular stroke volumes determined by magnetic resonance imaging. *European Journal of Nuclear Medicine* **11**, A18.

Underwood, S. R., Rees, R. S. O., Savage, P. E., Klipstein, R. H., Firmin, D. N., Fox, K. M., Poole-Wilson, P. A. & Longmore, D. B. (1986). Assessment of regional left ventricualr function by magnetic resonance. *British Heart Journal* **56**, 334–340.

Yamori, Y. (1984). Development of the spontaneously hypertensive rat (SHR) and of various spontaneous rat models, and their implications. In *Experimental and Genetic Models of Hypertension*, vol. 4, ed. Jong, W. D., pp. 224–239. Elsevier, Amsterdam, New York, Oxford.

Young, A. A. & Axel, L. (1992). Three-dimensional motion and deformation of the heart wall: estimation with spatial modulation of magnetisation – a model-based approach. *Radiology* **185**, 241–247.

Acknowledgements

The authors thank Dr Herchel Smith for his generous endowment which supports the Herchel Smith Laboratory. R.G.W. also thanks The Wellcome Trust for his Research Training Studentship in Mathematical Biology. A.I.M.A. thanks the Karim Rida Said Foundation for scholarship support. In addition, the authors also thank Dr Jim Crowley and Dr Andrew Gates for useful discussions and computer analysis software. The authors are grateful to Professor Donald Longmore for very useful discussions and his advice on cardiac function. C.L.-H.H., T.A.C. and L.D.H. thank BBSRC and MRC-JREI. The authors are grateful for the technical assistance of Mr Cliff Bunch and Mr Simon Smith.

Corresponding author

C. L.-H. Huang: The Physiological Laboratory, Downing Street, Cambridge CB2 3EG, UK.

Email: clh11@cus.cam.ac.uk